Dielectric Resonator-Microstrip Interactive Circuit Analysis and Design Using Integral Equation Techniques

Masood Yousefi, *Student Member, IEEE,* and Sujeet K. Chaudhuri, *Senior Member, IEEE*

***Abstract*—Dielectric resonators (DR's) are widely used in microwave/millimeter-wave technologies. In this paper, the coupling between a dielectric resonator and a microstrip circuit is studied. To analyze this problem, an integral equation is developed for the current distribution on the microstrip circuit. The Green's function used in this integral equation is the Green's function of the field in a layered medium modified by adding a term corresponding to the DR-scattered field. This field is produced by equivalent electric and magnetic sources assumed to be on the DR's surface. An efficient numerical method is applied which gives an approximation of the field near the resonant frequency of the DR. The results clearly show the effect of the DR on the microstrip circuit's current distribution and provides a thorough insight into the coupling mechanism. The coupling parameters can be estimated from the current distribution. The efficiency of the method as well as its flexibility in dealing with a general configuration of the DR and microstrip circuit makes it promising for CAD applications.**

I. Introduction

IN ORDER to use a dielectric resonator (DR) in a microstrip circuit, the coupling characteristics of the DR to a nearby microstrip circuit as well as its resonant frequencies should be known. Few efforts have been made to analyze the coupling between a DR and a microstrip transmission line on a grounded dielectric substrate [1], [2]–[5] and moreover, most of them have been demonstrated for the simplest geometry of the metallization, i.e., a straight microstrip-line, in the vicinity of the DR. No general and systematic way has been established to analyze the effect of a DR on a printed circuit metallization with a general shape, except of course for highly time-consuming methods like the Finite Element Method which need extensive computational resources. In the literature, the DR's field has been assumed in the absence of metallization and then the coupling of this field to the propagating mode of the microstrip line has been studied [1], [2], [4]. Here, the DR and metallization have been considered simultaneously in an interactive fashion.

The general configuration of the problem is depicted in Fig. 1. As shown in this figure, a cylindrical DR with $\varepsilon = \varepsilon_d = \varepsilon_{rd}\varepsilon_0$ is mounted on a grounded dielectric substrate with $\varepsilon = \varepsilon_s = \varepsilon_{rs}\varepsilon_0$. To tune the DR's resonant frequency, a tuning plate may be installed over the structure (not shown in the figure). An arbitrarily shaped metallization is printed on the substrate in the vicinity of the DR. The metallization is assumed to be infinitely thin. We are interested in the effect of the DR on the current distribution on the metallization. The S matrix of the N-port circuit within the dashed border in Fig. 1 is then obtained from the current distribution. The frequency of operation is assumed to be near a specific resonant frequency of the DR. In this frequency range the currents on the metallization induce a strong reactive field in the DR, which in turn affects the current distribution on the microstrip. Therefore, there is a bilateral relation between the current on the metallization and the DR's scattered field. In the literature, this bilateral relation has been ignored to simplify the analysis, e.g., the DR's field has been assumed in the absence of metallization and then the effect of this field on the propagating mode of the microstrip line has been studied.

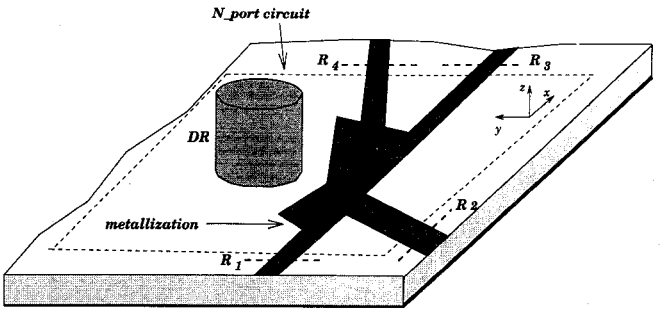

Fig. 1. A dielectric resonator (DR) coupled to a general N-port microstrip circuit on a grounded substrate.

A set of coupled integral equations can be formulated for the problem depicted in Fig. 1. The unknowns in these integral equations are the surface current density $\vec{J}_s$ over the microstrip metallization and the equivalent electric and magnetic sources on the surface of the DR, S_{DR}, denoted by $\vec{S}^d = (\vec{J}^d, \vec{M}^d)$. The metallization on the substrate is assumed to be infinitely thin.

The integral equations for the coupling problem can be obtained by applying the boundary conditions for the tangential electric field on the surface of the metallization, S_{met}, of Fig. 1, and the continuity of the tangential components of $\vec{E}$ and $\vec{H}$ on S_{DR} which are expressed as

$$-\hat{n} \times [\vec{E}_l(\vec{J}_s) + \vec{E}_l(\vec{S}^d)] = \hat{n} \times \vec{E}^{\text{ext}} \quad \text{on } S_{\text{met}} \tag{1}$$

$$\hat{n} \times [\vec{E}_l(\vec{J}_s) + \vec{E}_l(\vec{S}^d)] = -\hat{n} \times \vec{E}_0(\vec{S}^d) \quad \text{on } S_{DR} \tag{2}$$

$$\hat{n} \times [\vec{H}_l(\vec{J}_s) + \vec{H}_l(\vec{S}^d)] = -\hat{n} \times \vec{H}_0(\vec{S}^d) \quad \text{on } S_{DR}. \tag{3}$$

Manuscript received October 17, 1994; revised December 14, 1994.

The authors are with the Department of Electrical and Computer Engineering, University of Waterloo, Waterloo, Ont., Canada, N2L 3G1.

IEEE Log Number 9412053.

In (1)–(3) $\vec{E}_l(\vec{J}_s)$ denotes the electric field produced by $\vec{J}_s$ in the layered medium without the DR, $\vec{E}_0(\vec{S}^d)$ denotes the electric field produced by $\vec{S}^d$ in a homogeneous medium with $\varepsilon = \varepsilon_d$, and so on. The incident field denoted by $\vec{E}^{\text{ext}}$ is considered known and is only applied on the metallization.

The integral (1)–(3) can be written in the form

$$\begin{bmatrix} L^{mm} & L^{md} \\ L^{dm} & L^{dd} \end{bmatrix} \begin{bmatrix} \vec{J}_s \\ \vec{S}^d \end{bmatrix} = \begin{bmatrix} \hat{n} \times \vec{E}^{\text{ext}} \\ 0 \end{bmatrix} \tag{4}$$

where L^{mm}, L^{md}, L^{dm}, and L^{dd} are integral operators. The superscript m stands for metallization, and d stands for DR surface. The first and second superscripts on the L operators indicate the observation and source locations, respectively. Although the unknowns in the integral (4) are $\vec{J}_s$ and $\vec{S}^d$, one can eliminate $\vec{S}^d$ by combining the first and second equations of (4) and obtain

$$L^{mm}(\vec{J}_s) - L^{md}(L^{dd})^{-1}L^{dm}(\vec{J}_s) = \hat{n} \times \vec{E}^{\text{ext}}. \tag{5}$$

The first term of the left hand side of (5) is the conventional term used in the EFIE formulation for a planar metallization in a layered medium [6]. The second term is the electric field due to the presence of the DR (DR-scattered field). This term is the novel aspect of the formulation presented in this paper. Writing (5) in integral form yields

$$-\hat{n} \times \left\{ \int_{S_{\text{met}}} \overline{\overline{G}}_E(\vec{r}\|\vec{r}') \cdot \vec{J}_s(\vec{r}')\, ds' + \int_{S_{\text{met}}} \overline{\overline{G}}_2(\vec{r}\|\vec{r}') \cdot \vec{J}_s(\vec{r}')\, ds' \right\} = \hat{n} \times \vec{E}^{\text{ext}} \tag{6}$$

where $\overline{\overline{G}}_E$ is the dyadic electric field Green's function in the layered medium in the absence of the DR, $\overline{\overline{G}}_2$ is the DR-scattered Green's function to be determined, and $\hat{n}$ is the unit vector normal to S_{met}. The Green's function $\overline{\overline{G}}_2$ physically represents the response (scattered field) of the DR on the layered medium due to a unit current excitation.

Writing $\overline{\overline{G}}_E$ in terms of the well known vector magnetic potential $\overline{\overline{G}}_A$ and scalar electric potential G_V [6] defined in a multilayered medium at the operating frequency of ω, yields

$$\hat{n} \times \left\{ j\omega \int_{S_{\text{met}}} \overline{\overline{G}}_A(\vec{r}|\vec{r}') \cdot \vec{J}_s(\vec{r}')\, ds' + \nabla \int_{S_{\text{met}}} G_V(\vec{r}|\vec{r}')\rho_s(\vec{r}')\, ds' - \int_{S_{\text{met}}} \overline{\overline{G}}_2(\vec{r}|\vec{r}') \cdot \vec{J}_s(\vec{r}')\, ds' \right\} = \hat{n} \times \vec{E}^{ext}(\vec{r}) \vec{r} \in S_{\text{met}} \tag{7}$$

where ρ_s is the surface charge distribution on the surface of the metallization, S_{met}.

In Section II an efficient method will be presented to find an approximation for $\overline{\overline{G}}_2$ near one of the resonant frequencies of the structure so that (7) can be implemented numerically. The novelty of the proposed technique is the possibility of separating the effects of the metallization and the DR, and expressing the DR effect by an additive term. In Sections III and IV numerical results are presented for a stop-band and a pass-band DR-microstrip interactive circuit.

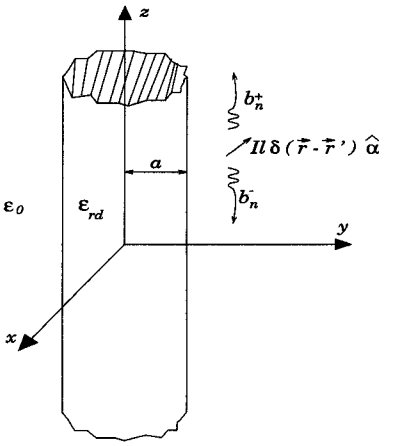

Fig. 2. Excitation of a dielectric rod by a current element.

II. Excitation of a DR by a Current Source

The $\overline{\overline{G}}_2$ term in (7) is the DR-scattered field induced by a current element. The procedure used here in solving for this field is as follows. First, suppose that the dielectric rod is infinite in both directions as shown in Fig. 2. The field for a current element providing the excitation to this rod can be obtained via the method described in [7], [8]. This field is in terms of a Fourier series in φ direction ($e^{jm\varphi}$). Fig. 3 is obtained from Fig. 2 by truncating the dielectric rod at $z = h$ and $z = h + d$. Each term of the Fourier series is reflected by the two grounded slabs at the top and bottom of the DR in Fig. 3. To simplify the formulation, the two grounded slabs are modeled by employing the Generalized Impedance Boundary Condition (GIBC) [9]. Therefore, the reflected waves are obtained by enforcing GIBC at $z = h$ and $z = h + d$. The advantage of GIBC technique over the conventional mode matching is that instead of considering the Helmholtz solution in three regions I, II, and III in Fig. 3, we consider only one region, i.e., the modes of the dielectric rod. The total scattered field is the sum of these terms over the index m. Of course, in a numerical computation one should truncate the summation. If the frequency of interest is near a resonant frequency of the DR, one of the terms with a specific azimuthal index of variation (m) would be expected to have the most significant contribution to the total field [8]. Since in practice a DR is always used near one of its resonant frequencies, we will consider only the azimuthal index corresponding to a specific DR mode and neglect the other terms of the series. Moreover, since a DR resonance is mostly due to constructive reflections of a specific guided mode at both ends of the rod, and the power stored in the DR is mostly in the fields of that mode, the radiation field and other non-resonant guided modes are neglected. This results in a very efficient estimation of the field bound to the DR near its resonant frequency. The $\overline{\overline{G}}_2$ field ensures the necessary boundary conditions at the cylindrical wall ($\rho = a$) of the DR. Due to the noninclusion of other modes of the dielectric rod, the boundary conditions at $z = h$ and $z = h + d$ is satisfied approximately.

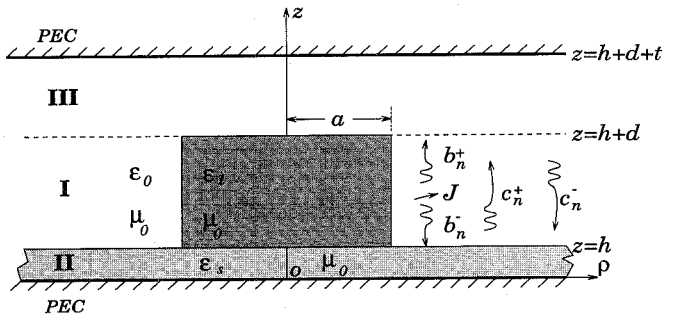

Fig. 3. A DR mounted on a grounded substrate and under a tuning plate, excited by a unit electric current dipole.

In reference to Fig. 2 for a current element denoted by

$$\vec{J}(\vec{r}) = Il\delta(\vec{r} - \vec{r}')\alpha \tag{8}$$

all of the TE^z field components can be obtained from H_z written in the form

$$H_z = \sum_{n=1}^{N_g} [b_n^+ H_{z0n}^+ + b_n^- H_{z0n}^-] + H_z^{(R)} \tag{9}$$

where $H_z^{(R)}$ is the radiation field of the dielectric rod [9], and $H_{z0n}^{\pm}$ represents the TE$_{0n}$ guided mode of the dielectric rod defined by

$$H_{z0n}^{\pm} = e^{\mp j\beta_{0n}(z-h)} \begin{cases} J_0(\xi_{0n}\rho) & \rho < a \\ \dfrac{J_0(\xi_{0n}a)}{K_0(\zeta_{0n}a)} K_0(\zeta_{0n}\rho) & \rho > a \end{cases} \tag{10}$$

and ζ_{0n}, ξ_{0n}, and β_{0n} are the solutions of the associated characteristic equation

$$-\frac{J_1(\xi_{0n}a)}{\xi_{0n}} = \frac{K_1(\zeta_{0n}a)}{\zeta_{0n}K_0(\zeta_{0n}a)} J_0(\xi_{0n}a) \tag{11}$$

with

$$\xi_{0n}^2 + \beta_{0n}^2 = k_d^2 = \varepsilon_{rd}k_0^2, \tag{12}$$

$$-\zeta_{0n}^2 + \beta_{0n}^2 = k_0^2. \tag{13}$$

In (9), $b_n^{\pm}$ (associated with waves traveling in $\pm z$ directions, respectively) are obtained [8] as

$$b_n^{\pm} = \hat{\alpha} \cdot \hat{\varphi}'[E_{\varphi 0n}^{\mp}]_{\vec{r}} = \vec{r}' \Big[4\pi\omega\mu_0\beta_{0n}a^2 J_0(\xi_{0n}a) \cdot \left(\frac{J_0(\xi_{0n}a)}{2} - \frac{J_1(\xi_{0n}a)}{\xi_{0n}a}\right)\left(\frac{1}{\zeta_{0n}^2} + \frac{1}{\xi_{0n}^2}\right)\Big]^{-1} \tag{14}$$

where

$$E_{\varphi 0n}^{\pm} = e^{\mp j\beta_{0n}(z-h)} \begin{cases} \dfrac{-j\omega\mu_0}{\xi_{0n}} J_1(\xi_{0n}\rho) & \rho < a \\ \dfrac{j\omega\mu_0 J_0(\xi_{0n}a)}{\zeta_{0n}K_0(\zeta_{0n}a)} K_1(\zeta_{0n}\rho) & \rho > a. \end{cases} \tag{15}$$

Equation (9) gives H_z as a summation of TE^z guided modes and a radiation field and describes the TE^z part of the field induced by a current element in an infinitely long dielectric rod. The total excited field, $\overline{\overline{G}}_2$, in Fig. 3 is composed of the original $b_n^+ H_{z0n}^+ + b_n^- H_{z0n}^-$ field in (9) and the fields reflected from the slabs in Fig. 3, i.e., $c_n^+ H_{z0n}^+$ and $c_n^- H_{z0n}^-$. Therefore, the total field is

$$H_{z0n}^{\text{tot}} = \begin{cases} (b_n^+ + c_n^+)H_{z0n}^+ + c_n^- H_{z0n}^- & z > z' \\ c_n^+ H_{z0n}^+ + (b_n^- + c_n^-)H_{z0n}^- & z < z' \end{cases} \tag{16}$$

where z and z' refer to observation and source points, respectively. The unknown coefficients $c_n^{\pm}$ in (16) are then obtained by enforcing GIBC at $z = h$ and $z = h + d$. H_{z0n}^{tot} acts as a potential function for all the components of the excited resonant field, $\overline{\overline{G}}_2$. For further details the reader is referred to [8] and [9].

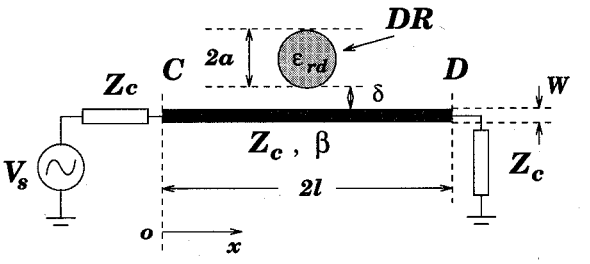

Fig. 4. A DR coupled to a straight microstrip line to realize a stop-band filter.

With the knowledge of all the required Green's functions, (7) can be solved numerically by the method of moments (MoM) for the unknown current distribution on the metallization. For the results presented in this paper, the current and charge distributions on the metallization are segmented into current cells and charge nodes, respectively. Two-dimensional pulse functions are used as the basis functions. The resultant set of equations is then solved for the unknown current distribution $\vec{J}_s$. Since the method was developed for CAD applications, a special technique was implemented to compute the elements in the MoM matrix very efficiently [8]. The additive term $\overline{\overline{G}}_2(\vec{r}|\vec{r}')$ in (7) provides the effect of the presence of the DR on the current distribution. Applications of the numerical scheme in the DR-microstrip circuit coupling analysis is demonstrated in Sections III and IV.

III. Analysis of a Band-Stop DR Filter

One of the DR-microstrip interactive circuits commonly used in microwave technology is shown in Fig. 4. This circuit has been studied by the MoM. This configuration is suitable for exciting TE$_{0n\delta}$ modes of the DR. For this group of modes, the electric field has only E_φ component. Therefore, they can have a strong coupling to the axial microstrip current in the vicinity of the DR. The TE$_{01\delta}$ mode widely used in DR-microstrip circuits has been selected for the test.

The current distribution obtained by the MoM solution of (7) is used to find the S matrix of the circuit in Fig. 4 as a function of frequency. This S matrix can be attributed to an equivalent circuit model of the DR-microstrip interaction (at least over a narrow band around the resonance frequency). One choice of equivalent circuit for the configuration under consideration here is depicted in Fig. 5. One may then choose the parameters of this equivalent circuit (L, C, G, and Q_E) to fit the MoM generated S matrix. This circuit model can then be used in the design and analysis of a more complicated microwave circuit.

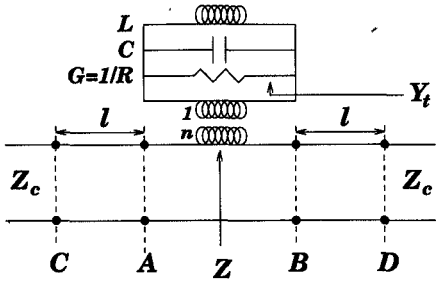

Fig. 5. An equivalent circuit for the stop-band filter.

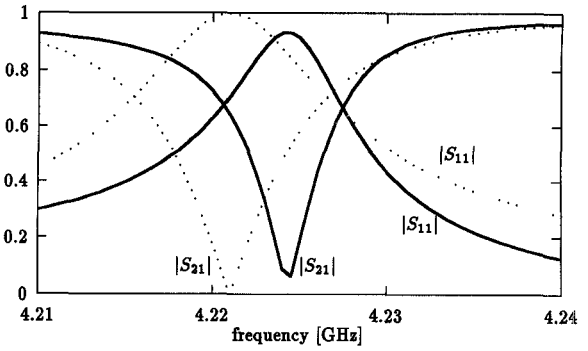

Fig. 6. $|s_{11}|$ and $|s_{21}|$ from C to D for $N_w = 1$ and $\delta = 1$ mm. Solid line: MoM, dotted line: experimental from [1]. The results of the MoM have been shifted down by about 40 MHz (1% shift in resonant frequency) to make the comparisons easy.

This procedure is demonstrated in this section using the case of a band-stop DR filter.

In Fig. 5, the DR has been modeled by a parallel GLC circuit. L and C represent the reactive field of the DR, while $G = 1/R$ is the model for loss in the DR which consists of dielectric and radiation loss. Thus, for a DR with low loss, high ε_r material, G is usually very small and may be ignored.

The GLC circuit Fig. 5 has an admittance of

$$Y_t = G(1 + ju) \tag{17}$$

where

$$u \triangleq Q_0\left(\frac{\omega}{\omega_0} - \frac{\omega_0}{\omega}\right). \tag{18}$$

Q_0 is the internal quality factor of the DR defined by $Q_0 = \omega_0 CR$ and $\omega_0 = 1/\sqrt{LC}$ is the angular resonant frequency of the GLC circuit. For ω close to ω_0, one may write u as

$$u \cong 2Q_0\frac{\delta\omega}{\omega_0}, \tag{19}$$

where $\delta\omega = \omega - \omega_0$.

The S matrix from A to B in Fig. 5 is described by

$$s_{11} = \frac{n^2}{n^2 + 2Z_cY_t}, \tag{20}$$

$$s_{21} = \frac{2Z_cY_t}{n^2 + 2Z_cY_t}. \tag{21}$$

One can obtain all of the resonance and coupling information from the above S matrix. To characterize the coupling more clearly and in an engineering fashion, note that

$$\frac{s_{21}}{s_{11}} = \frac{1}{\beta_c} + ju_e \tag{22}$$

where

$$\frac{1}{\beta_c} = \frac{2Z_c}{n^2}G \tag{23}$$

and

$$u_e \cong 2Q_E\frac{\delta\omega}{\omega_0}. \tag{24}$$

In the above equations β_c is called the *coupling parameter*, and $Q_E \triangleq Q_0/\beta_c$ is called the *external quality factor* of the DR. By combining (22) and (24) one can get Q_E in terms of the S matrix as

$$Q_E = \frac{\omega_0}{2}\frac{\partial}{\partial\omega}\left[\mathrm{Im}\left(\frac{s_{21}}{s_{11}}\right)\right]_{\omega=\omega_0} \tag{25}$$

Equation (25) has been employed in [1] to find Q_E of the DR in Fig. 4 from the measured S matrix around the resonant frequency. For numerical evaluation of Q_E, the current distribution obtained by MoM is used to calculate s_{21} and s_{11}. The numerical value of Q_E is then determined from (25).

Circuit specifications: For the numerical demonstrations the line has been taken long enough to assure that the (spatial) transient effect of the DR coupling has decayed sufficiently at the far ends. This has been assured by observing that varying the length of the line does not affect the S matrix except, of course, for a simple phase shift. The fixed specifications of the circuit are $\varepsilon_{rs} = 2.62$, $h = 1.57$ mm, $H = 150$ mm, $a = 8.19$ mm, $d = 5.44$ mm, $\varepsilon_{rd} = 27$, $W = 4.9$ mm, and l= 39 mm, where ε_{rs}, h, and H are the substrate relative dielectric permittivity, thickness and the height of the upper PEC shield, and a, d, and ε_{rd} are the DR's radius, height, and relative dielectric permittivity, respectively. The number of charge cells in the length and width directions are designated by N_l and N_w, respectively. W and l are defined in Fig. 4. For the numerical tests here we have fixed $N_l = 52$, and N_w varies from 1 to 3.

The s_{11} and s_{21} obtained by the MoM are shown in Figs. 6 and 7. For comparison, the measured data (ω_0 and Q_E) from [1] has been used to obtain the parameters L and C of the equivalent circuit shown in Fig. 5. One may note that $|s_{11}|$ obtained by MoM does not reach the value 1.0. This is due to the radiation and surface wave loss of the microstrip circuit (automatically included in the Green's functions $\overline{\overline{G}}_A$ and G_V). But the same curve derived from the experimental data reaches the value 1.0. This is because no value was reported for G in [1], and thus in the circuit model of Fig. 5 it was neglected ($G = 0$).

If only a guided mode is assumed in the DR, the resonant frequency calculated with this method is within few percent of the exact value. Since the DR has a very narrow-band resonance and its quality factor is typically of the order of several hundreds to several thousands, any small error in resonant frequency makes the comparison on the same diagram difficult. Therefore, the results of the MoM have been shifted down by about 40 MHz (1% shift in resonant frequency) to make the comparisons easy in Figs. 6, 7, 13, and 14.

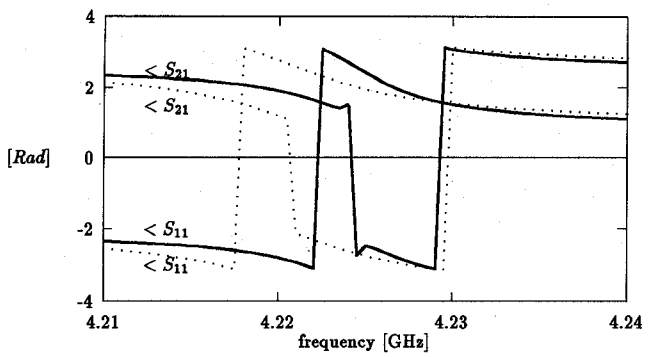

Fig. 7. $<s_{11}$ and $<s_{21}$ from C to D for $N_w = 1$ and $\delta = 1$ mm. Solid line: MoM, dotted line: experimental from [1]. The results of the MoM have been shifted down by about 40 MHz (1% shift in resonant frequency) to make the comparisons easy.

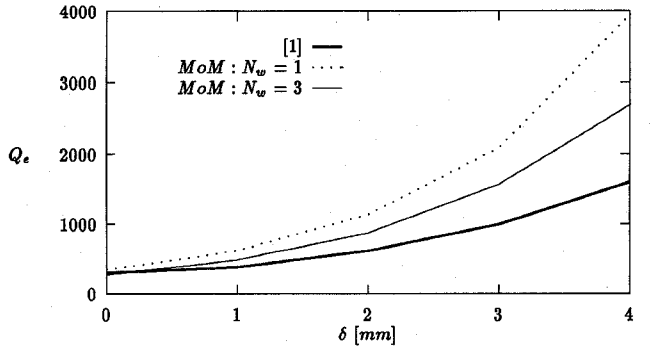

Fig. 8. Q_E versus δ for the DR-microstrip coupling.

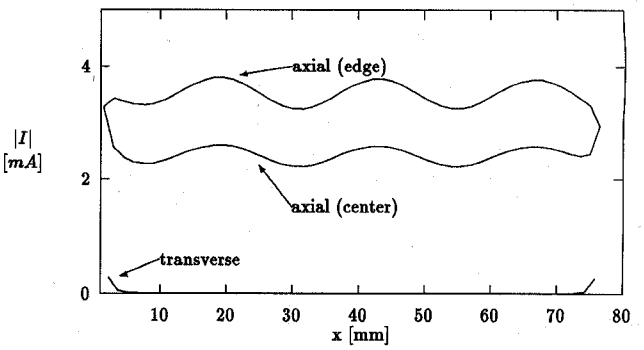

Fig. 9. The current distribution on the line near the resonant frequency, for $N_w = 3$ and $\delta = 1$ mm in the absence of DR. x is the axial distance on the line.

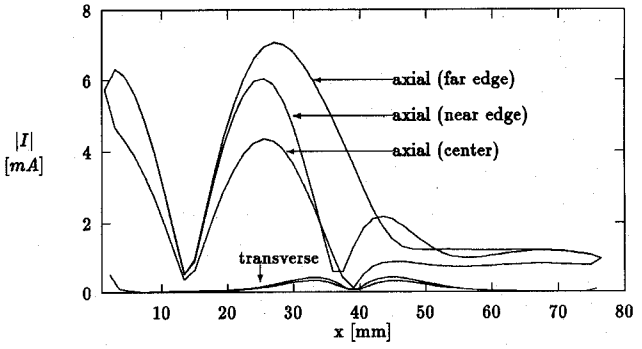

Fig. 10. The current distribution on the line near the resonant frequency, for $N_w = 3$ and $\delta = 1$ mm, in the presence of DR. x is the axial distance on the line.

Q_E has been computed versus δ, the distance between DR and line, and is shown in Fig. 8. One of the curves corresponds to $N_w = 1$, i.e., no segmentation along transverse direction. The other curve corresponds to $N_w = 3$. It can be observed that discretizing the microstrip line along transverse direction improves the result. This will be explained in more detail later.

Fig. 8 also shows that for large separation between DR and microstrip line, the assumption of only the resonant guided mode and not accounting for the DR radiation field underestimates the resonant field and the coupling. Therefore, the Q_E of the circuit is overestimated for large distances. However, DR's are mostly used in the immediate vicinity of the nearby metallization and this method is able to predict their Q_E with good accuracy.

The MoM results for the current distribution on the line for $N_w = 3$ with/without the DR are shown in Figs. 9 and 10. By discretizing the metallization in width, the current distribution is allowed to vary along transverse direction. As can be observed in Fig. 9, in the absence of DR, the axial currents at edges of the line are equal and larger in amplitude than the axial current at the center of the line. This stems from the fact that the structure is symmetric along transverse direction and, the axial current is singular at the line edges. Also note that the transverse currents are negligible compared to the axial current, which is one of the features of the fundamental mode of a microstrip line.

By adding the DR to the structure at one side of the line, the transverse symmetry of the current is no longer maintained. Fig. 10 shows that at the coupling area, which is near $x =$ 39 mm, the current distribution is tilted toward the DR. This asymmetry rapidly disappears at points away from the DR. Moreover, the transverse current in this case is no longer negligible. Fig. 10 shows that at the transition region—the region between the symmetric and asymmetric current distribution—the transverse current is increased to redistribute the axial current toward a symmetric one. These observations are further appreciated by eliminating the transverse current from the scene, which produces the results shown in Fig. 11. In this figure the asymmetry in the axial current does not tend to vanish. This observation has been confirmed by testing it on longer lines. The transverse distribution of the axial current has an oscillatory behavior and does not stabilize. Thus, inclusion of the transverse current is important for accurate modeling of the coupling.

In summary, letting the axial current distribution vary along transverse direction needs a transverse current. Part of the DR-microstrip line coupling is achieved by this transverse current. This results in a stronger coupling or equivalently a lower Q_E, which justifies the behavior of the Q_E curves with respect to N_w in Fig. 8.

IV. Analysis of a Band-Pass DR Filter

As the second example, the circuit in Fig. 12 has been studied. Since the two lines are relatively far from each other, one expects that energy is not transferred from input to output at frequencies far from the resonant frequency. As

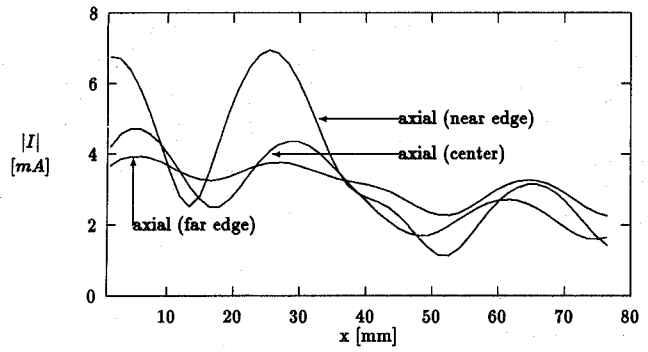

Fig. 11. The current distribution on the line near the resonant frequency, for $N_w = 3$ and $\delta = 1$ mm, in the presence of DR and with eliminating the transverse current. x is the axial distance on the line.

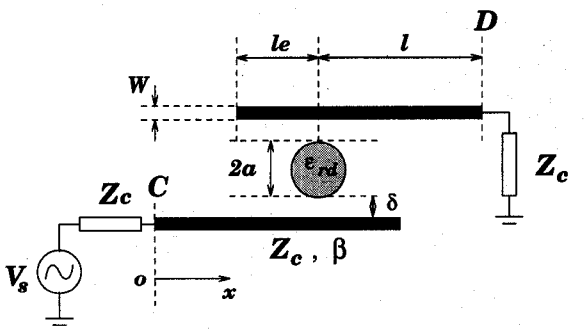

Fig. 12. A band-pass DR filter.

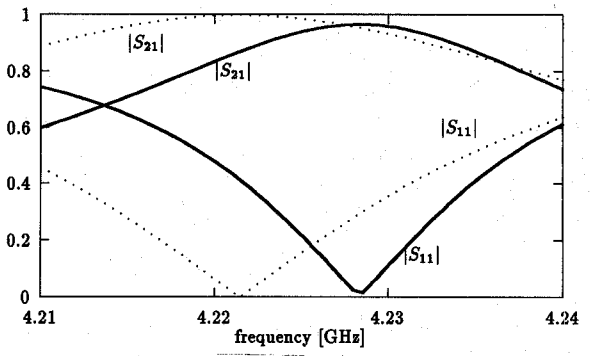

Fig. 13. $|s_{11}|$ and $|s_{21}|$ from C to D for $N_w = 1$ and $\delta = 1$ mm. Solid line: MoM, dotted line: experimental from [1]. The results of the MoM have been shifted down by about 40 MHz (1% shift in resonant frequency) to make the comparisons easy.

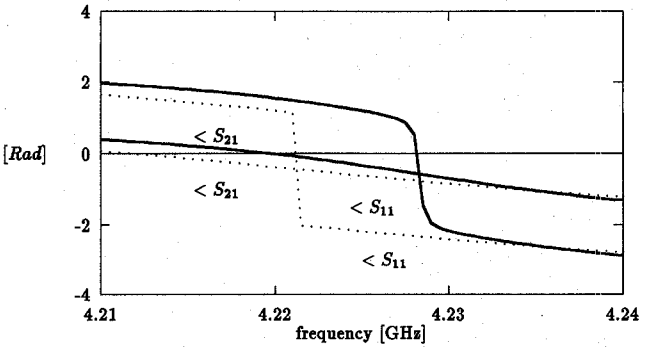

Fig. 14. $<s_{11}$ and $<s_{21}$ from C to D for $N_w = 1$ and $\delta = 1$ mm. Solid line: MoM, dotted line: experimental from [1]. The results of the MoM have been shifted down by about 40 MHz (1% shift in resonant frequency) to make the comparisons easy.

the operating frequency approaches the resonant frequency, the DR links the two ports. Therefore, this circuit is expected to act like a band-pass filter. For simplicity, the circuit has been assumed symmetric, so that the input and output ports are interchangeable.

The circuit specifications have been assumed to be the same as those of the band-stop filter of the previous example, except that $l = 50$ mm and $l_e = 12$ mm An equivalent circuit can be proposed in a similar way as in the previous circuit [8].

For $\delta = 1$ mm and $N_w = 1, s_{11}$ and s_{21} are computed and shown in Figs. 13 and 14. These results are compared with those obtained by the simulation of its equivalent circuit with experimental parameters extracted from [1]. By comparing these results with those of the previous example, i.e., Figs. 6 and 7, one realizes that s_{11} and s_{21} have much broader bandwidth for this circuit. This is because, in Fig. 12, the resonator sees an additional load from the upper line. Moreover, the resistive value of this load is almost half of that of the previous example.

The input and output line current distributions at the resonant frequency were observed numerically. In the absence of DR, the input current has a standing wave pattern due to the open circuit reflection at the end of the input line. On the output line, no current is induced. By including the DR to the structure, the standing wave pattern at the input line is replaced with a traveling wave pattern indicating that the power is transferred from input line to the output line. The induced current on the output line also has a traveling wave pattern, as a result of the absorption of energy by the matched output load.

V. Conclusion

In this paper we have developed a versatile and efficient tool for the analysis and design of dielectric resonator-microstrip interactive circuits. A mixed potential integral equation (MPIE) was used to solve the interaction between the DR and the microstrip circuit. The coupling between the DR and a nearby metallization with an arbitrary shape has been modeled by solving this integral equation. Method of Moments (MoM) was employed to solve the integral equation. The method has led to the direct calculation of the S matrix of the circuit as well as its coupling parameters and has given a clear qualitative insight into the behavior of DR-microstrip interactions. The flexibility of the method to analyze a DR on a generally shaped metallization, and its computational efficiency has been demonstrated through the analysis of a band-stop and a band-pass DR-microstrip filter. The calculated S matrices of the DR filters are presented. Also the current distributions on the metallization with and without the DR show the coupling mechanism of the DR-microstrip circuit very clearly. The external quality factor, Q_e of a DR coupled to a straight microstrip line is computed and compared with measured data. Also it is shown that a part of the coupling is due to the transverse current of the microstrip line which is usually neglected. Numerical results also show that the presence of the DR disturbs the symmetry of the microstrip line's axial current, and demonstrates the role of the transverse current in the

redistribution of the axial current toward a symmetric one. The developed tool can predict the behavior of complicated DR-microstrip interactive circuits and aids one in the determination of the optimum parameters of the DR/metallization part of the circuit. Use of this method in the design of a band-pass filter with two DR's has been demonstrated [8]. The time-efficiency of the method in conjunction with its versatility makes it an attractive choice for CAD software development.

REFERENCES

[1] F. M. van Heeswyk, "A generalized method for the analysis of coupling between a dielectric resonator and microstrip circuits," Master's thesis, University of Waterloo, Ontario, 1989.

[2] P. Guillon, B. Byzery, and M. Chaubet, "Coupling parameters between a dielectric resonator and a microstripline," *IEEE Trans. Microwave Theory Tech.*, vol. MTT-33, pp. 222-226, Mar. 1985.

[3] A. E. Atia and R. R. Bonetti, "Coupling of cylindrical dielectric resonators to microstrip lines," in *1981 Int. Microwave Symp. Dig.*, Los Angeles, p. 167, June 15–19, 1981.

[4] R. R. Bonetti and A. E. Atia, "Analysis of microstrip circuits coupled to delectric resonators," *IEEE Trans. Microwave Theory Tech.*, vol. MTT-29, pp. 1333–1337, Dec. 1981.

[5] P. Guillon and S. Mekerta, "Dielectric resonator bandstop filter," in *1981 Int. Microwave Symp. Dig.*, Los Angeles, June 15–19, 1981, p. 170.

[6] J. R. Mosig, "Integral equation technique," in *Numerical Techniques for Microwave and Millimeter-Wave Passive Structures*, T. Itoh, Ed. New York: Wiley, 1989, pp. 133–213.

[7] W. C. Chew, *Waves and Fields in Inhomogeneous Media*. New York: Van Nostrand Reinhold, 1990.

[8] M. Yousefi, "Analysis of the coupling between a dielectric resonator and a microstrip circuit," Ph.D. thesis, Dept. of Elec. and Comp. Eng., Univ. of Waterloo, Waterloo, Ontario, 1994.

[9] M. Yousefi, S. K. Chaudhuri, and S. Safavi-Naeini, "GIBC formulation for the resonant frequencies and field distribution of a substrate mounted dielectric resonator," *IEEE Trans. Antennas Propagat.*, vol. 42, pp. 38–46, Jan. 1994.

Masood Yousefi (S'85) was born in Tehran, Iran, in 1960. He received the B.Sc. and M.Sc. degrees in electrical engineering from the University of Tehran in 1986 and 1988, respectively. He completed his Ph.D. degree at the University of Waterloo, Canada, in the field of microwaves, in 1994.

His research interests include electromagnetics, numerical simulation of microwave circuits, and data structures and algorithms in numerical solution of electromagnetic problems.

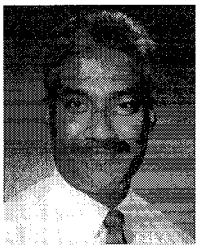

Sujeet K. Chaudhuri (M'79–SM'85) was born in Calcutta, India, on August 25, 1949. He graduated with the B.E. (honors) degree in electronics engineering from BITS/Pilani, and the M.Tech. degree in electrical communications engineering from IIT/Delhi, India in 1970 and 1972, respectively. He received the M.A.Sc. degree in microwave engineering and the Ph.D. degree in electromagnetic theory in 1973 and 1977, respectively, at the University of Manitoba, Canada.

In 1977 he joined the University of Waterloo, Canada, where he is currently a Professor and the Chair of the Electrical and Computer Engineering Department. He has also held a Visiting Associate Professorship in the EECS Department of the University of Illinois at Chicago in 1981 and 1984, and a Visiting Professorship at the National University of Singapore in 1990 through 1991. He has been involved in contract research and consulting work with several Canadian and U.S. industries and government research organizations. His current research interests are in guided-wave/electrooptic structures, planar microwave structures, dielectric resonators, optical and EM imagining, and the fiber based broadband network.

Dr. Chaudhuri is a member of URSI Commission B, and Sigma Xi.